Conf-820601--22

FRACTURE-MECHANICS DATA DEDUCED FROM THERMAL-SHOCK AND RELATED EXPERIMENTS WITH LWR PRESSURE-VESSEL MATERIAL*

CONF-820601--22

DE82 018162

R. D. Cheverton[a] S. E. Bolt[a]
D. A. Canonico[b] P. P. Holz[a]
S. K. Iskander[c] R. K. Nanstad[d]
W. J. Stelzman[a]

Introduction

Pressurized water reactors (PWRs) are susceptible to certain types of hypothetical accidents that can subject the reactor pressure vessel to severe thermal shock, that is, a rapid cooling of the inner surface of the vessel wall [1–3]. The thermal-shock loading, coupled with the radiation-induced reduction in the material fracture toughness, introduces the possibility of propagation of preexistent flaws and what at one time were regarded as somewhat unique fracture-oriented conditions. Thus, an investigation, both analytical and experimental, of flaw behavior in PWR pressure vessels under thermal-shock loading conditions was in order. In 1973 the Nuclear Regulatory Commission (NRC) established a thermal-shock task at Oak Ridge National Laboratory (ORNL) as a part of the Heavy-Section Steel Technology (HSST) Program, and since that time several postulated reactor accidents have been analyzed to discover flaw behavior trends; seven intermediate-scale thermal-shock experiments with steel cylinders have been conducted; and corresponding materials characterization studies have been performed. Flaw behavior trends and related fracture-mechanics data deduced from these studies are the subject of this paper.

*Research sponsored by the Office of Nuclear Regulatory Research, U.S. Nuclear Regulatory Commission, under Interagency Agreements 40-551-75 and 40-552-75 with the U.S. Department of Energy under contract W-7405-eng-26 with the Union Carbide Corporation.

[a]Oak Ridge National Laboratory, P.O. Box Y, Oak Ridge, TN 37830.
[b]Combustion Engineering, Inc. 911 West Main St., Chattanooga, TN 37402.
[c]Union Carbide Corp., Nuclear Div., P.O. Box P, Oak Ridge, TN 37830.
[d]Oak Ridge National Laboratory, P.O. Box X, Oak Ridge, TN 37830.

Analysis of the LBLOCA

Reactor accidents of concern with regard to thermal shock are those that allow cool water to come in contact with the inner surface of the reactor vessel, where the fast-neutron fluence and thus the radiation-induced reduction in fracture toughness in the wall is a maximum. A PWR accident of this type is the large-break loss-of-coolant accident (LBLOCA), which has the potential for imposing a very severe thermal shock on the inner surface of the reactor pressure vessel [1–3]. Because of this potential the LBLOCA was selected for analysis during the early phases of the thermal-shock program. The intent of the analysis was to determine the apparent magnitude of the thermal-shock problem, discover flaw behavior trends, and use this information in scoping an experimental program, if needed.

The specific transient considered for the LBLOCA consisted of a step change in coolant temperature from 288 to 21°C and a step change in pressure from normal operating pressure to one atmosphere. Additional input to the analysis included a typically high concentration of copper (0.34%) [4], which enhances the radiation-induced reduction in fracture toughness [5]; an initial RTNDT of −18°C; and a fluence of 1.5×10^{19} n/cm^2 at the inner surface, which corresponds to ∿32 EFPY for a reactor with a typically low fluence rate and to ∿10 EFPY for a reactor with a typically high fluence rate.

The type of flaw considered in the analysis was a long, axially oriented, inner-surface crack, which has a greater potential than other types for deep penetration of the wall. Flaw behavior during the LBLOCA was analyzed using linear elastic fracture mechanics (LEFM) [6], and the stress intensity factors (K_I) were calculated with a finite-element technique [7]. The static crack initiation toughness (K_{Ic}) and static crack arrest toughness (K_{Ia}) were taken from ASME Section XI, and the shift in the nil-ductility reference temperature

(ΔRTNDT) due to fast neutron fluence and including the effects of copper was taken from Reg. Guide 1.99, Rev. 1 [5].

Results of the analysis for the LBLOCA are illustrated in Figs. 1 and 2. Figure 1 shows typical temperature, resultant thermal stress, fluence, K_{Ic} and K_{Ia} distributions through the wall, at a particular time in the transient, and the K_I values for long axial flaws of different assumed depths. As indicated, the positive gradient in temperature, coupled with the steep attenuation of the fluence and the tendency for fracture toughness to increase with temperature, results in a steep positive gradient in fracture toughness. However, K_I also increases with crack depth, and for the particular case analyzed it appears that both a shallow and a deep flaw would initiate ($K_I = K_{Ic}$) and then arrest ($K_I = K_{Ia}$). It is also of interest to note that arrest must take place with K_I increasing with crack depth rather than decreasing. When measuring K_{Ia} in the lab, K_I is usually decreasing with increasing crack depth.

If the crack depths corresponding to the intersections of the K_I curve with the K_{Ic} and K_{Ia} curves are plotted as a function of the time in the transient at which the intersections (initiation and arrest events) take place, a set of curves, referred to as the critical-crack-depth curves, is obtained which indicates the behavior of the flaw during the entire transient. The critical-crack-depth curves for the LBLOCA case, shown in Fig. 2, indicate that a flaw will propagate in a stepwise fashion. If the flaw is effectively blunted, requiring a K_I value greater than K_{Ic} for initiation, or if it is very shallow, so that the lower portion of the initiation curve is applicable, relatively long crack jumps would take place, and this might introduce dynamic effects at arrest that could make the usual static analysis inadequate [8].

Figure 3 also includes the locus of points for $K_I = (K_I)_{max}$, that is, $dK_I/dt = 0$, a curve that is referred to as the warm prestress curve (WPS).

For times less than those indicated by the WPS curve K_I increases with time, and for times to the right of the WPS curve K_I decreases with time. Under this latter condition ($dK_I/dt < 0$) a crack presumably could not initiate even with $K_I >> K_{Ic}$ [9]. As indicated in Fig. 2, WPS presumably would limit crack propagation to about 38% of the wall thickness, whereas without WPS the flaw would extend ∿95% of the way through the wall. Assuming WPS to be effective, the maximum calculated value of K_I/K_{Ic} for the final crack depth ($a/w = 0.38$), was ∿2.0.

Thermal-Shock Experiments

The analysis of the LBLOCA not only revealed a potential for deep penetration of a preexistent flaw but also indicated a somewhat unique set of fracture-mechanics conditions associated with thermal-shock loading. Thus, an experimental program was in order.

The purpose and scope of the thermal-shock experiments was to investigate the flaw behavior trends identified in the analysis of the LBLOCA. More specifically, the scope was to include (1) an examination of the validity of LEFM for thermal shock, (2) a demonstration of WPS, (3) a demonstration of arrest in a rising K_I field, (4) an attempt to introduce dynamic effects by means of a long crack jump, and (5) a demonstration of the inability of a fast-running crack to penetrate the wall as the terminus to a long and deep crack jump.

Thus far, seven thermal-shock experiments have been conducted [10–13]. The last three, TSE-5, 5A and 6, are of greatest importance and are the ones discussed in this paper. Test conditions for these experiments are summarized in Table 1.

In order to simulate reactor conditions as well as was deemed reasonable and yet attain conditions necessary for obtaining meaningful data, the experiments were conducted with rather large-diameter, thick-walled cylinders fabricated from steel having a chemical composition typical for PWR pressure vessels. Cladding was omitted, and 25 mm or more of surface material was removed, following the quench-in-water portion of the heat treatment, to effectively eliminate residual stresses and an undesirable gradient in toughness [14]. The length selected for the test cylinders was effectively infinite in terms of the effect of the free ends on K_I, and the initial flaw extended the full length of the cylinder, thus permitting an accurate two-dimensional analysis of K_I (about two-thirds of the length of the cylinder was free of end effects). The initial flaw was on the inner surface, was of uniform depth, and was generated by means of the electron-beam-weld technique [15].

The thermal shock was applied to the inner surface only and was severe enough and at low enough temperature to nearly compensate for the absence of radiation damage. Additional control over fracture toughness was achieved through the selection of an appropriate tempering temperature for the test cylinder material.

To achieve the desired thermal shock the test cylinder, initially at a temperature of 96°C, was submerged in liquid nitrogen (−197°C). The ends and outer surface of the cylinder were heavily insulated, while the inner surface was coated with a thin layer (∿0.8 mm) of a "rubber cement" type of material that suppressed film boiling and promoted nucleate boiling, which provided the necessary high heat transfer coefficient. Experimental data retrieved during the experiment included temperature distributions through the wall, the time of initiation-arrest events, static crack opening displacement (COD) and COD vs time during a run-arrest event.

The times of events were indicated by step changes in the COD data and by ultrasonic (UT) instrumentation that looked at the tip of the flaw. The depth of the flaw was determined by examination of the fracture surface, by UT measurements and by the COD data, after correlating COD to crack depth by means of a posttest finite-element analysis. This same correlation was used to convert COD vs time, which was recorded on a fast-phenomena recorder, to crack depth vs time and thus crack-tip velocity during a run arrest event.

The measured temperature distributions were used in the posttest fracture mechanics analysis of the experiments, thus eliminating uncertainties in an otherwise necessary thermal analysis. The temperature distributions and measured crack depths corresponding to the actual times of initiation-arrest events were used to calculate the corresponding critical values of K_I. These K_I values were then used in judging the validity of LEFM for the test conditions by comparing these critical K_I values with K_{Ic} and K_{Ia} values measured in the lab with appropriate small specimens. If the values agreed reasonably well, then LEFM was considered to be reasonably valid.

Materials Characterization Studies

The test-cylinder material specified for the thermal-shock experiments was A508 with class-2 chemistry (see Table 2), and tempering temperatures were selected that would result in the desired toughness curves (K_{Ic} vs T). Although toughness data were generally available for A508 class-2 material, an adequate design and posttest analysis of each thermal-shock experiment required fracture toughness data specifically for each of the three test cylinders. Pretest data for the three cylinders, which were taken from a single long forging, were obtained using prolongations of each cylinder as a source of material for laboratory specimens. In some cases, following the experiment, the test-cylinder material itself was used.

Material properties measured in the lab included the yield and ultimate strengths, Charpy and drop-weight data, static crack-initiation toughness (K_J) and static crack arrest toughness (K_{Ia}), all as a function of temperature. Battelle Columbus Labs (BCL) obtained the K_{Ia} and some of the K_J data; a few K_J specimens were tested by the United States Naval Ship Research and Development Center (USNSRDC); and the rest of the material testing was performed at ORNL.

The K_J data were obtained using compact specimens, and for each test cylinder at least ten specimens were tested at each of several temperatures of interest. A few specimens were side-grooved (BCL) [16] and a few were spring loaded (USNSRDC) [17] in an effort to reduce the scatter in the K_J data. The K_{Ia} data were obtained with compact, wedge-loaded, crack arrest specimens (25 x 150 x 150 mm), and relatively few K_{Ia} values were measured. For all lab K_{Ia} and K_J measurements the orientation of the specimens relative to a test cylinder was such that the flaw orientation was the same for the specimens and cylinders.

During the K_J testing, ductile tearing preceded brittle fracture in many of the compact specimens, and because of this an attempt was made to obtain J_{Ic} values, using the unloading compliance technique. However, satisfactory J-R curves could not be obtained in most cases because the temperature range of interest to the thermal-shock experiments was too low (mid-transition and lower). To derive K_J values from the conventional test data the J integral was calculated using the energy to maximum load, and K_J was determined from $K_J^2 = EJ$. In all cases the specimens failed by cleavage fracture, and in most cases failure occurred before limit load.

Appropriate tempering temperatures for the thermal-shock experiments were selected by first obtaining K_J curves for a range of tempering temperatures

(594–704°C) and then comparing curves selected on the basis of experiment-design calculations with the lab curves. An indication of the variation in toughness with tempering temperature is illustrated in Fig. 3 [18], which is a plot of the test temperature required for a Charpy energy of 68 J and for a Charpy-specimen lateral expansion of 0.89 mm as a function of tempering temperature. (Charpy data were obtained for a broader range of tempering temperatures, including quench only.) The 68-J curve shows a slight increase in test temperature up to a tempering temperature of ∿594°C and then a drop in test temperature from 100 to −10°C, the latter value corresponding to a tempering temperature of 704°C. The room-temperature yield strength for tempering temperatures ≤594°C was ∿700 MPa, and for the highest tempering temperature (704°C) it was ∿500 MPa.

Toughness Data for TSE-5 and 6

The TSE-5 and 6 test cylinders were tempered at 613°C, resulting in an RTNDT of 66°C and room-temperature yield and ultimate strengths of 710 and 850 MPa, the latter value being substantially in excess of that permitted for class-2 material. For TSE-5 three compact-specimen sizes (0.4T, 1T and 2T) were used to obtain K_J data, while for TSE-6, only 1T specimens were used. The limited amount of testing for the TSE-6 cylinder was considered adequate for comparing properties of the TSE-5 and 6 cylinders, which were taken from opposite ends of the original forging, and for extending the low-temperature end of the toughness curve.

All of the lab K_J and K_{Ia} data for the TSE-5 and 6 test cylinder prolongations are presented in Fig. 4. It is evident that data from the two prolongs agree very well, but there is large scatter in the K_J data throughout the transition region for each of the three specimen sizes. For example, at 82°C

the range in K_J values, as measured with eight 1T and eight 2T specimens, was 125 to 310 MPa $m^{1/2}$, but both specimen sizes yielded the same lower-bound value.

Figure 5 also indicates that some of the lower K_J values are valid K_{Ic} values (in accordance with ASTM Standard E-399) [19], and that there is substantial scatter in these data as well. For instance, at −18°C the scatter in valid data is ±28%, and at −73°C it is ±32%.

As would be expected, the K_{Ia} data are generally lower than the K_J data but do overlap the lower bound of the latter data. The scatter in the K_{Ia} data is substantial but not as large as that for the K_J data.

Toughness Data for TSE-5A

The test cylinder for TSE-5A was tempered at 679°C, which resulted in an RTNDT of 10°C and room-temperature yield and ultimate strengths of 605 and 740 MPa. The latter value is only slightly in excess of that permissible for A508 class-2 material.

The K_J data were obtained with 1T compact specimens only, and, as shown in Fig. 5, the scatter was similar to that for the TSE-5 and 6 material. It is also observed that K_J data obtained by Battelle Columbus Laboratories (BCL), using side-grooved specimens (10% per side), and by USNSRDC, using a spring in series with the specimen to increase the compliance of the loading system, did not alter the scatter trend.

Because of the large amount of scatter observed in the K_J data for the TSE-5, 5A and 6 materials, extensive Charpy testing was conducted for the TSE-5A test cylinder and its prolongation to see if similar scatter would be obtained. The results in Fig. 6 indicate that the scatter in Charpy data is about the same as that in the K_J data and that there is no detectable difference in Charpy data between the test cylinder and its prolongation.

Discussion of Results

Valid K_{Ic} data were obtained for the TSE-5 and 6 test cylinders over most of the temperature range of interest, permitting a meaningful comparison of lab data with K_{Ic} values deduced from the thermal-shock experiments. However, to obtain the valid data a rather large number of lab specimens had to be tested at each test temperature because many values of K_J were not valid as a result of the large scatter in the data. This had no bearing on the interpretation of the thermal-shock experiments, but it does suggest a problem in terms of obtaining valid K_{Ic} values with a reasonable number of small specimens. A satisfactory solution to this problem is of particular importance in connection with obtaining adequate toughness data from the limited number of surveillance specimens in operating reactors.

It is of interest to note that the valid K_{Ic} data obtained for the TSE-5 and 6 test cylinders correspond to a lower-bound region of the scatter band, and, as will be discussed in more detail later, the K_{Ic} values deduced from TSE-5 and 6 tended to fall within this region. To this extent the long flaws in TSE-5 and 6 behaved in accordance with the lower bound of the lab K_J data.

No valid K_{Ic} values were obtained for the TSE-5A test cylinder, using the compact specimens. However, based on the results of TSE-5 and the TSE-5 materials characterization studies, it was believed that the lower-bound K_J values obtained by testing ten 1T specimens at each of several temperatures would be adequate for the purpose of designing the experiment, and this was the case.

Results of Thermal-Shock Experiments

TSE-5

Thermal-shock experiment TSE-5 was designed for a stepwise propagation of the flaw with WPS limiting the number of initiation-arrest events to three

and with crack arrest taking place in a rising K_I field. However, the design was based on inadequate toughness data and on a misconception of crack behavior, resulting in the selection of a tempering temperature that was too low. As a result conditions for a convincing demonstration of WPS and arrest in a rising K_I field were not achieved. Nevertheless, there were three initiation-arrest events. They took place at 1.75, 2.95 and 3.24 min into the transient, and the crack jump distances were 20, 61 and 26 mm, respectively, for a total penetration of 80% of the wall. The K_I values and crack-tip temperatures corresponding to the initiation and arrest events are shown in Table 3, and the same K_I values are compared with the lab small-specimen data in Fig. 7. As indicated by the data in Figs. 4 and 7, the TSE-5 K_I values corresponding to the three initiation events are close to the lower bound of the lab K_J data. However, the K_I value for the second initiation event is relatively high, indicating an effectively blunted crack tip, and this accounts for the relatively long crack jump. This is illustrated in Fig. 8, which is a posttest set of critical-crack-depth curves that was obtained by using a smooth toughness curve through the K_{Ic} data points corresponding to the first and third initiation events. The figure includes the actual path of events (crack depth vs time), and it is observed that the point corresponding to the second initiation event falls to the right of the calculated initiation curve, which was forced to go through the points corresponding to the first and third initiation events. Thus, the second point falls in a region of the figure where, based on the use of a smooth fracture toughness curve, K_I is greater than K_{Ic}, in which case a relatively long crack jump and thus possibly dynamic effects would be expected.

As indicated in Fig. 8, a smooth curve (crack arrest curve) can be drawn through the experimental points corresponding to the three arrest events. If

it is assumed that there were no significant dynamic effects associated with the smaller crack jumps (first and third events), then the absence of a discontinuity in the arrest curve indicates that there were no significant dynamic effects associated with the second event.

A comparison of the crack-arrest data is also included in Fig. 7, and as indicated the agreement between the K_{Ia} values deduced from TSE-5 and those measured in the lab with small specimens is reasonably good; that is, the TSE-5 values fall within the scatter band of the small-specimen data. If there were dynamic effects that resulted in a K_I value at arrest greater than the calculated static value, then the K_{Ia} value deduced from TSE-5 on the basis of a static calculation would be less than the actual value. As shown in Fig. 7 the K_{Ia} value deduced from TSE-5 for the second event is high relative to the values for the first and third events. Thus, a dynamic effect is not apparent.

The output from two COD gages located near midlength of the test cylinder was recorded with fast-phenomena recording equipment for the long crack jump that occurred during TSE-5, and the results are shown in Fig. 9. As indicated, the maximum COD rate was at the beginning of the event. Thereafter, the rate gradually decreased to zero as the crack arrest event was approached. There are no indications of an overshoot in COD and thus in K_I at arrest, which is another indication that dynamic effects at arrest were negligible. By relating crack depth to COD using a static finite-element analysis [7], it was possible to estimate crack-tip velocity from COD rate. In this manner the maximum crack-tip velocity was estimated to be $\sim$120 m/s, which is low compared to values measured in the lab with crack arrest specimens ($\sim$700 m/s) [20]. This difference is probably due to the fact that the ratio of the initiating K_I value to K_{Ic} was larger for the lab test than for the second event during TSE-5.

In summary, based on the observation that the critical values of K_I for crack initiation during TSE-5 were close to, though somewhat greater than, the lower bound of lab small-specimen (1T and 2T-CS) data, the lower bound being valid in accordance with ASTM E399 [19], the results of TSE-5 indicate that LEFM is valid under severe thermal-shock loading conditions for both shallow and deep long flaws in large structures. Furthermore, the crack-arrest toughness data deduced from TSE-5 were consistent with the lab K_{Ia} data, and the long crack-jump event during TSE-5 appeared to have negligible dynamic effects associated with it.

TSE-5A

TSE-5A was designed to achieve the goals originally set forth for TSE-5. Thus, as implied by the results of TSE-5 and subsequent materials characterization studies, it was necessary to specify a higher tempering temperature (greater toughness) for TSE-5A than for TSE-5. By doing so, the test goals for TSE-5A were met.

During TSE-5A, there were four initiation-arrest events; a fifth initiation event was prevented by WPS; the final crack depth was about fifty percent of the wall thickness; the maximum value of K_I/K_{Ic} for the final crack depth was 2.3, satisfying a requirement for a convincing demonstration of WPS; and the first arrest event took place in a rising K_I field. The actual times, crack depths, crack-tip temperatures and the posttest calculated K_I values corresponding to the initiation and arrest events are shown in Table 4, and a comparison of the K_{Ic} and K_{Ia} values deduced from TSE-5A are compared with the corresponding design curves in Fig. 10. As indicated in Fig. 10, the four K_{Ic} and K_{Ia} values deduced from TSE-5A are shifted ∿22K to the right of the K_{Ic} and K_{Ia} design curves. Once again a lower-bound K_J behavior was exhibited, but this time both the K_{Ic} and K_{Ia} values deduced from the thermal-shock experiment

were lower than the small-specimen lower-bound data. This is attributed to the apparent low probability of obtaining plane-strain toughness values for the test cylinder material using 1T-CS specimens.

If the toughness curves deduced from TSE-5A (dashed curves in Fig. 10) are used in a posttest analysis of the experiment, the set of critical-crack depth curves shown in Fig. 11, which includes the actual path of events, is obtained. These curves show that a fifth initiation event would have taken place had it not been for WPS, and that the maximum value of K_I/K_{Ic} finally achieved (~14 min) for the final crack depth was 2.3.

The first arrest event during TSE-5A took place, although just barely, in a rising K_I field, as illustrated in Fig. 12, and, as indicated in Fig. 10, the corresponding K_{Ia} value does not appear to be out of line with those values obtained for the three other arrest events, which took place in a falling K_I field.

TSE-6

The most recent thermal-shock experiment, TSE-6, was designed to examine the possibility of a fast-running crack penetrating the outer surface of the test cylinder under conditions for which an LEFM static analysis indicated that the crack would stop short of full penetration. The desired single, long crack jump and deep penetration were to be achieved by reducing the wall thickness (relative to that for TSE-5 and 5A) to reduce the stiffness of the wall and thus increase $dK_I/d(a/w)$, and by using low-toughness material (the same as for TSE-5). The final design of TSE-6 was based on a fracture toughness curve that was drawn through the K_{Ic} values deduced from TSE-5 for the first and third initiation events (Fig. 7). The corresponding critical-crack-depth curves, shown in Fig. 13, indicated that starting with a shallow flaw (a/w = 0.1) the desired conditions could be met.

During TSE-6 there were two initiation-arrest events instead of one, but the second crack jump was nevertheless reasonably long ($\Delta a/w = 0.66$), and arrest took place deep in the wall ($a/w = 0.93$). Data pertaining to the events are summarized in Table 5, and the K_I values corresponding to the events are compared to the lab small-specimen and TSE-5 data in Fig. 7. The K_I value corresponding to the first initiation event is below the design curve and is even a little less than the lower bound of the lab data, while the K_I value for the second initiation event is somewhat above the design curve but not as much above as the K_I value for the second initiation event in TSE-5. Also, the K_I value for the first arrest event was close to the lower bound of the lab K_{Ia} data, while that for the second arrest event was close to the upper bound. If the actual dynamic K_I value corresponding to the second arrest event were significantly greater than the calculated static value, then the static value would tend to be low relative to the lab K_{Ia} data. Since this was not the case, a dynamic effect is not discernible on the basis of a comparison of K_{Ia} values.

Statically calculated values of K_I as a function of crack depth for the times at which the two initiation-arrest events took place are shown in Fig. 14. Also included are the points on the curves corresponding to the initiation and arrest events. It is observed that the first arrest event took place in a rising K_I field. Since the critical K_I value for this event falls within the scatter band of the lab K_{Ia} data, a variation in K_{Ia} due to arrest taking place in a rising K_I field is not apparent.

Comparison of Toughness Data with ASME Section XI K_{Ic} and K_{Ia} Curves

The test cylinders for TSE-5, 5A, and 6 did not satisfy A508 class 2 specifications with regard to strength, which, as a result of lower-than-normal tempering temperatures, was much too high for TSE-5 and 6 and only slightly too

high for TSE-5A. Even so, it is of interest to compare the toughness data for these cylinders with the ASME Section XI K_{Ic} and K_{Ia} vs T – RTNDT curves, and this has been done in Fig. 15. As indicated, when normalized with T – RTNDT, all of the data fall to the left of the respective ASME curves.

Conclusions

Tentative conclusions arrived at on the basis of the HSST thermal-shock experiments are as follows:

1. LEFM appears to be valid for both shallow and deep long flaws in thick-walled steel cylinders under severe thermal-shock loading conditions.
2. The scatter in K_J data obtained from 1T and 2T-CS specimens for A508 class-2 chemistry steel tempered at 613 or 679°C is large (~±50%) throughout the transition region.
3. Long flaws in a thick-walled cylinder of the above material tend to behave in accordance with the lower bound of the lab K_J and K_{Ia} data.
4. Crack arrest will take place in a rising K_I field ($dK_I/da > 0$) in accordance with lab K_{Ia} data.
5. Since K_{Ia} values deduced from the thermal-shock experiments, using a static analysis, fell within the scatter band of lab data, it appears that dynamic effects at arrest were negligible.
6. Crack initiation will not take place under thermal-shock loading conditions while K_I is decreasing with time even though $(K_I/K_{Ic}) >> 1$ (a WPS phenomenon).
7. Since all toughness data related to the thermal-shock experiments fell above the respective ASME Section XI K_{Ic} and K_{Ia} vs T – RTNDT curves, it appears that the later curves are conservative.

Nomenclature

a	Crack depth in wall of cylinder
a_c	Critical crack depth
a/W	Fractional crack depth
E	Neutron energy
E	Young's modulus
F	Fast-neutron fluence (E > 1 MeV)
F_o	Fast-neutron fluence at inner surface of vessel wall
K_I	Mode I stress intensity factor
K_{Ia}	Static crack arrest toughness
K_{Ic}	Static crack initiation toughness
K_J	Fracture toughness obtained by J integral
RTNDT	Nil ductility reference temperature
$RTNDT_o$	Initial (zero fluence) RTNDT
T	Temperature
TSC-1, 2, 3	Test cylinders used in thermal-shock experiments TSE-5, 5A and 6
t	Time
w	Wall thickness of cylinder
1T, 2T-CS	One-inch and two-inch compact specimens

Acknowledgments

This research was sponsored by the Office of Nuclear Regulatory Research, U.S. Nuclear Regulatory Commission (NRC). The authors wish to acknowledge the direction and encouragement provided by Milton Vagins, NRC, and Grady Whitman, director of the ORNL HSST program.

References

1. Tuppeny, W. H., Jr., Siddall, W. F., Jr., and Hsu, L. C., *Thermal Shock Analysis on Reactor Vessels Due to Emergency Core Cooling System Operation*, Combustion Engineering, Inc., Report A-68-9-1, March 15, 1968.

2. Hutto, R. C., Morgan, C. D., and Van Der Sluys, W. A., *Analysis of the Structural Integrity of a Reactor Vessel Subjected to Thermal Shock*, Babcock & Wilcox Power Generation Division, Topical Report BAW10018, May 1969.

3. Ayres, D. J., and Siddall, W. F., Jr., *Finite Element Analysis of Structural Integrity of a Reactor Pressure Vessel During Emergency Core Cooling*, Combustion Engineering Report A-70-19-2, January 1970, also presented at Petroleum Mechanical Engineering Pressure Vessel and Piping Conference, Denver, Colorado, Sept. 1970.

4. P. N. Randall (USNRC), personal communications.

5. U.S. Nuclear Regulatory Commission, "Effects of Residual Elements on Predicted Radiation Damage to Reactor Pressure Vessel Materials," *Regulatory Guide 1.99*, Rev. 1, Sept. 16, 1976.

6. Rolfe, S. T., and Barsom, J. M., *Fracture and Fatigue Control in Structures, Applications of Fracture Mechanics*, Prentice-Hall, Inc., 1977.

7. Iskander, S.K., *Two Finite-Element Techniques for Computing Mode I Stress Intensity Factors in Two- and Three-Dimensional Problems*, ORNL/NUREG/CSD/TM-14, Feb. 1981.

8. Hahn, T. G., and Kanninen, M. F., *Fast Fracture and Crack Arrest*, ASTM STP 627, American Society for Testing and Materials, 1977, p. 411.

9. Loss, F. J., Gray, A. A., Jr., and Hawthorne, J. R., *Significance of Warm Prestress to Crack Initiation During Thermal Shock*, Naval Reserch Laboratory, Washington, DC, NRL/NUREG 8165, Sept. 1977.

10. Cheverton, R. D., Iskander, S. K., and Bolt, S. E., *Applicability of LEFM to the Analysis of PWR Vessels Under LOCA-ECC Thermal Shock Conditions*, NUREG/CR-0107 (ORNL/NUREG-40), Oak Ridge National Laboratory, Oak Ridge, TN, Oct. 1978.

11. Cheverton, R. D., "Thermal Shock Investigations," *Heavy-Section Steel Technology Program Quart. Prog. Rep. July–September 1979*, ORNL/NUREG/TM-370, pp. 52–80.

12. Cheverton, R. D., "Thermal Shock Investigations," *Heavy-Section Steel Technology Program Quart. Prog. Rep. October–December 1980*, ORNL/NUREG/TM-437, March 1981, pp. 37–50.

13. Cheverton, R.D., "Thermal Shock Investigations," *Heavy Section Steel Technology Program Quart. Prog. Rep. October–December 1981* (in preparation).

14. Canonico, D. A., et al., *Assessment of Materials Technology of Pressure Vessels and Piping for Coal Conversion System*, ORNL-5238, Aug. 1978.

15. Holz, P. P., *Flaw Preparations for HSST Program Vessel Fracture Mechanics Testing; Mechanical-Cyclic Pumping and Electron-Beam Weld-Hydrogen Charge Cracking Schemes*, NUREG/CR-1274 (ORNL/NUREG/TM-369), Oak Ridge National Laboratory, Oak Ridge, TN, May 1980.

16. Rosenfield, A. R., and Shetty, D. K., "Lower-Bound Toughness of a Reactor-Vessel Steel," *Engineering Fracture Mechanics*, Vol. 14, pp. 833–842, 1981.

17. Vassilaros, M. (USNSRDC), letter to D. A. Canonico (ORNL), March 1981.

18. Canonico, D. A., and Stelzman, W. J., "Thermal-Shock Temper Study," *Heavy-Section Steel Technology Program Quart. Prog. Rep. April–June 1979*, NUREG/CR-0980 (ORNL/NUREG/TM-347), Oct. 1979, p. 68.

19. "Plane Strain Fracture Toughness of Metallic Materials," ASTM E 399-78, *Annual Book of ASTM Standards, Part 31*, American Society for Testing and Materials, Philadelphia, PA, 1978.

20. Cheverton, R. D., et al., "Application of Crack Arrest Theory to a Thermal Shock Experiment," *Crack Arrest Methodology and Applications*, ASTM STP 711, Hahn, G. T., and Kanninen, M. F., eds., American Society for Testing and Materials, 1980, pp. 392–421.

Table 1. Summary of test conditions for thermal-shock experiments TSE-5, 5A and 6

Parameter	Experiment		
	TSE-5	TSE-5A	TSE-6
Cylinder dimensions, mm			
Outside diameter	991	991	991
Wall thickness	152	152	76
Length	1220	1220	1220
Cylinder material			
Designation	A508, class-2 chemistry		
Tempering temperature, °C	613	679	613
Tempering time, hr	4	4	4
RTNDT, °C	66	10	66
Flaw (initial)			
Orientation	Axial	Axial	Axial
Length, mm	1220	1220	1220
Depth, mm	16	11	7.6
Method of generation	Electron-beam weld plus hydrogen charging		
Thermal shock			
Initial temp. of cylinder, °C	96	96	96
Quench medium	LN_2	LN_2	LN_2

Table 2. Chemical composition for TSE-5, 5A and 6 test cylinders

	Composition, wt %								
	C	Mn	P	S	Si	Cr	Ni	Mo	V
Heat analysis[a]	0.23	0.77	0.008	0.006	0.27	0.39	0.81	0.63	0.03
Check analysis:									
Top	0.23	0.79	0.009	0.006	0.28	0.41	0.82	0.63	0.03
Bottom	0.18	0.76	0.007	0.004	0.29	0.40	0.79	0.63	0.03
ASME Specification SA-508 class 2[b]	0.27	0.50 / 1.00	0.012	0.015	0.15 / 0.40	0.25 / 0.45	0.50 / 1.00	0.55 / 0.70	0.05

[a]National Forge Heat 41-5655.

[b]Single values are maximum.

Table 3. Results of TSE-5

Time (s)	Event	a/w	T (°C)	K_I (MPa$\sqrt{m}$)
105	Init.	0.10	−9	79
	Arrest	0.20	36	86
177	Init.	0.20	−3	111
	Arrest	0.63	82	104
205	Init.	0.63	79	115
	Arrest	0.80	89	92

Table 4. Results of TSE-5A

Time (s)	Event	a/w	T (°C)	K_I (MPa$\sqrt{m}$)
78.5	Init.	0.076	−11	70
	Arrest	0.138	22	76
90.5	Init.	0.138	12	85
	Arrest	0.198	38	86
123.0	Init.	0.198	13	108
	Arrest	0.316	51	107
184.5	Init.	0.316	21	135
	Arrest	0.535[a]	67	130

[a]For this final crack depth $(K_I/K_{Ic})_{max}$ = 2.3 at ∿14 min.

Table 5. Summary of events for TSE-6

Time (s)	Event	a/w	T (°C)	K_I (MPa$\sqrt{m}$)
69	Init.	0.10	−12	46
	Arrest	0.27	34	63
137	Init.	0.27	−28	87
	Arrest	0.93	64	105

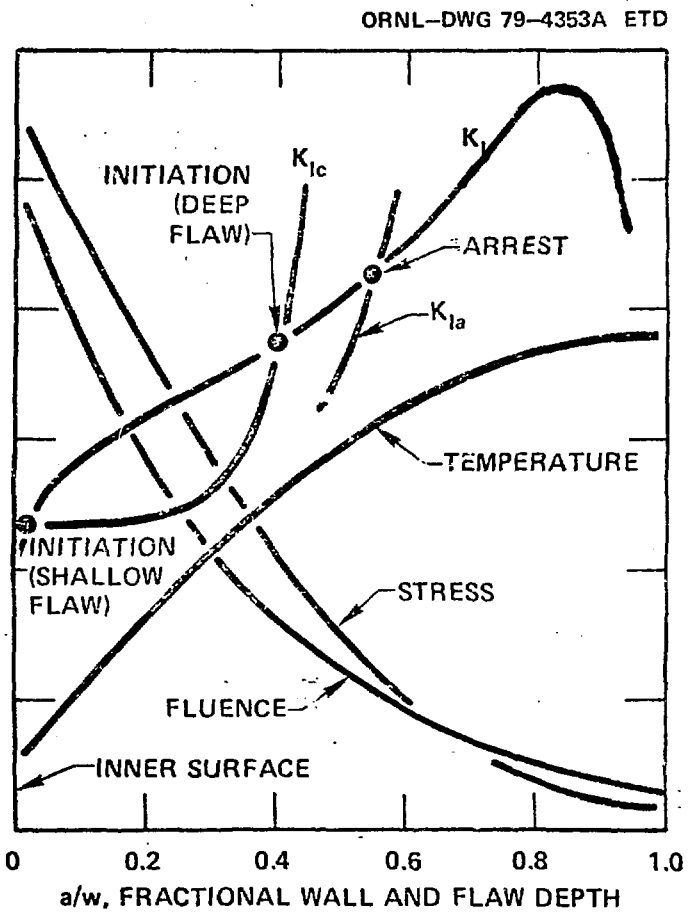

Fig. 1. Distribution of various fracture-mechanics related parameters through the wall of a PWR pressure vessel at a particular time in a LBLOCA.

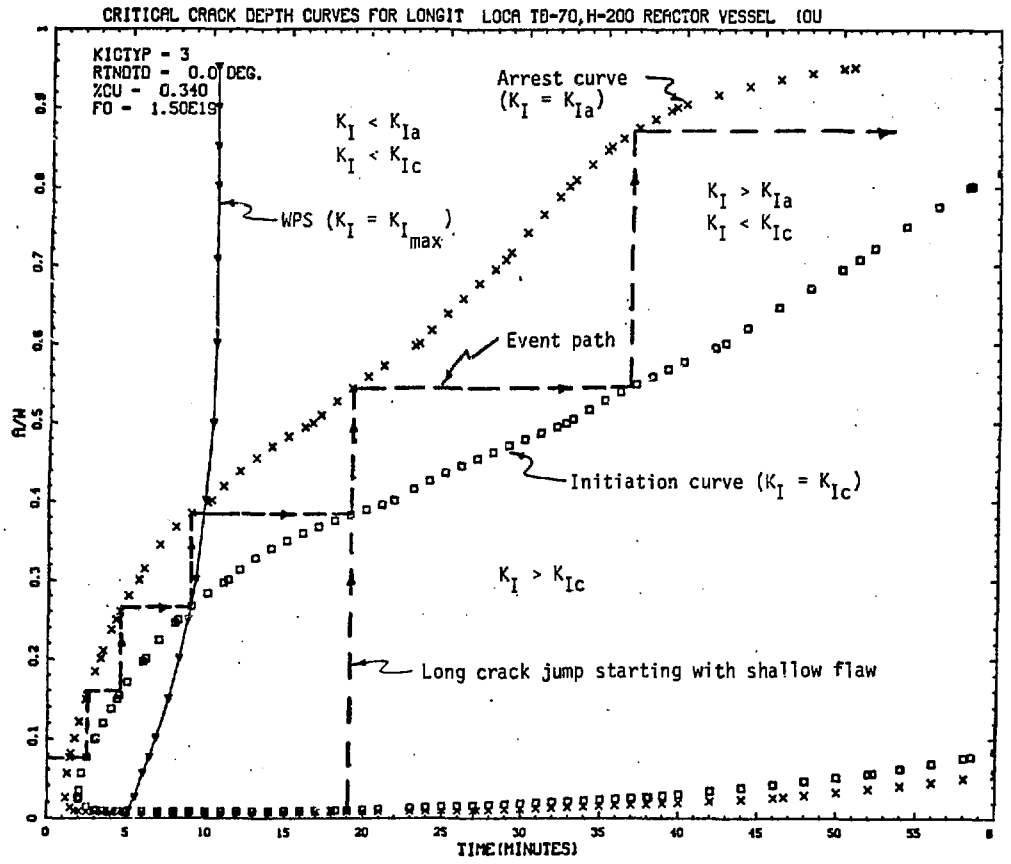

Fig. 2. Critical-crack-depth curves for the reference calculational model LBLOCA.

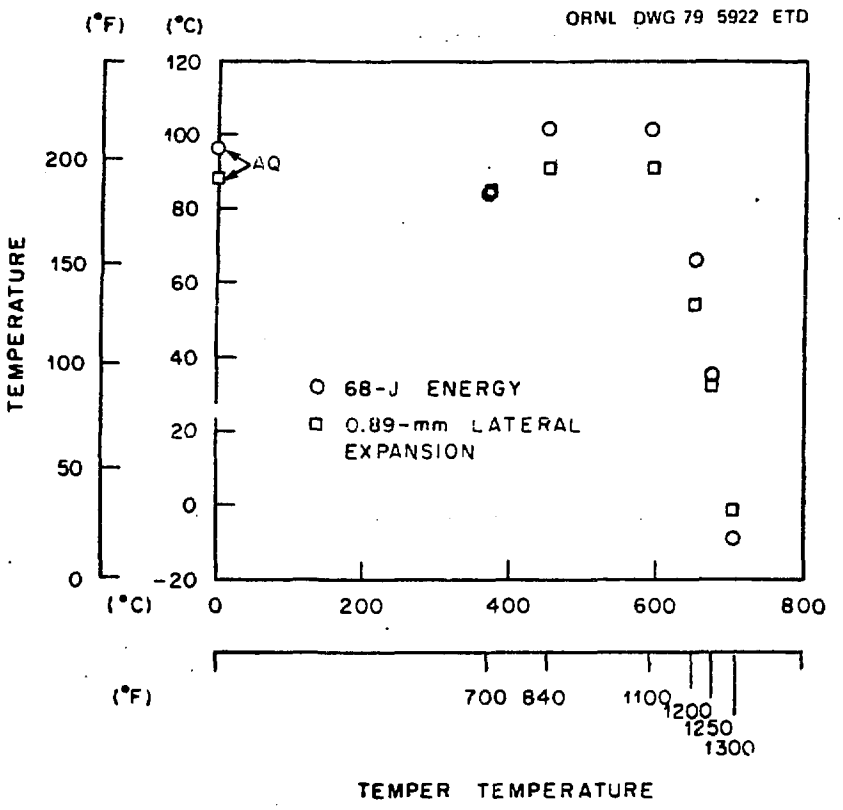

Fig. 3. Effects of tempering temperature on temperatures corresponding to CVN energy of 68 J and lateral expansion of 0.89 mm for TSE-5 test cylinder prolongation after tempering for 4 h and cooling in air.

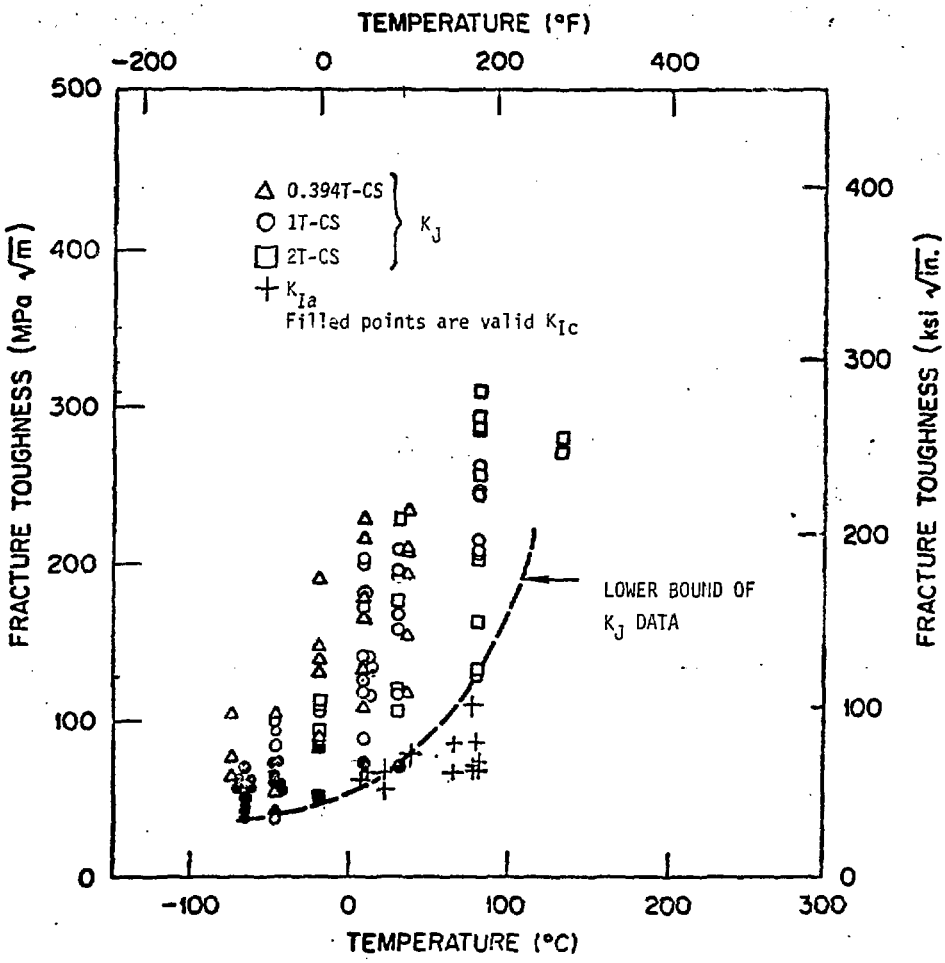

Fig. 4. K_J and K_{Ia} data obtained for TSE-5 and 6 test-cylinder prolongations.

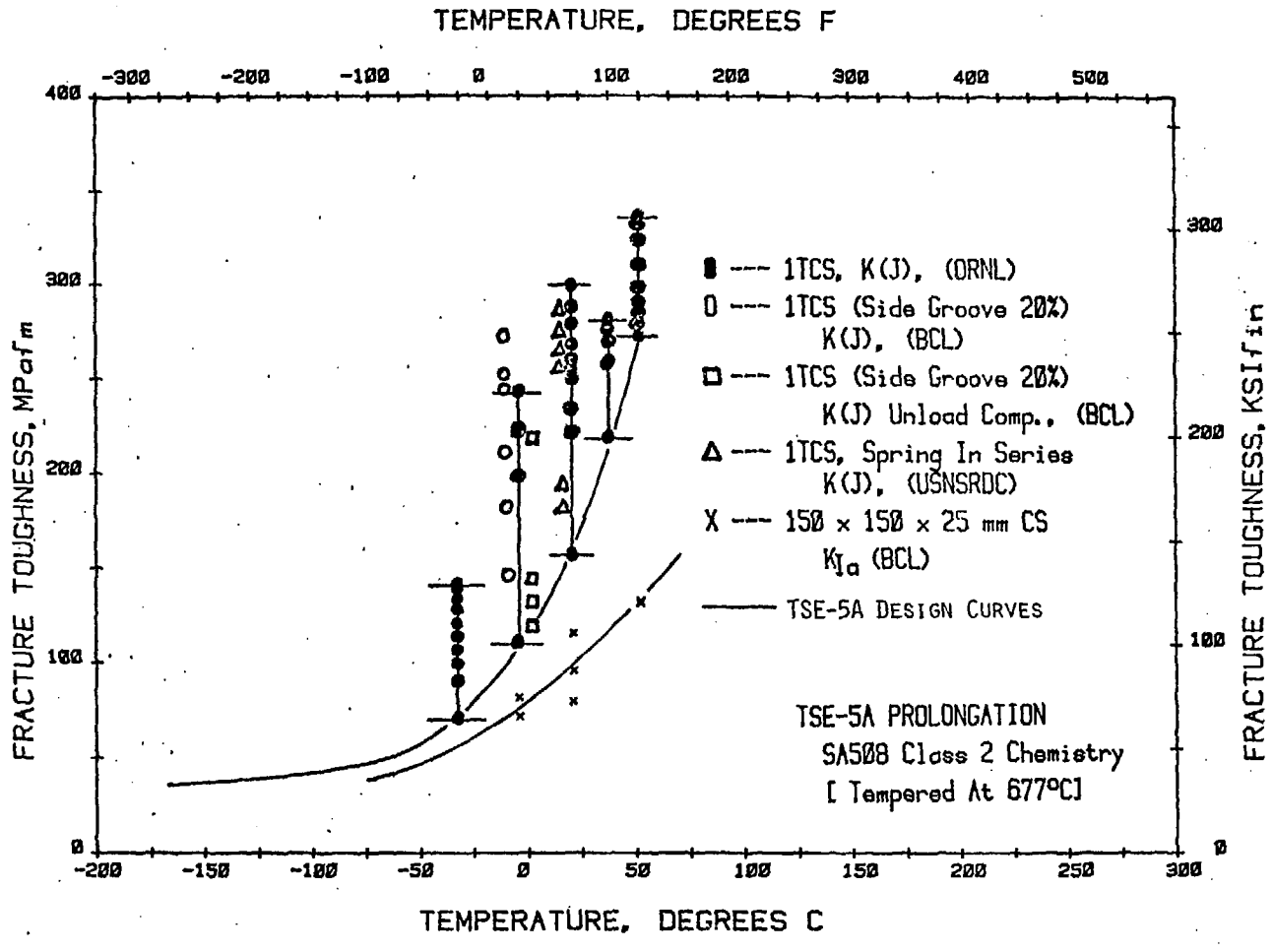

Fig. 5. Fracture toughness data for TSE-5A test-cylinder prolongation.

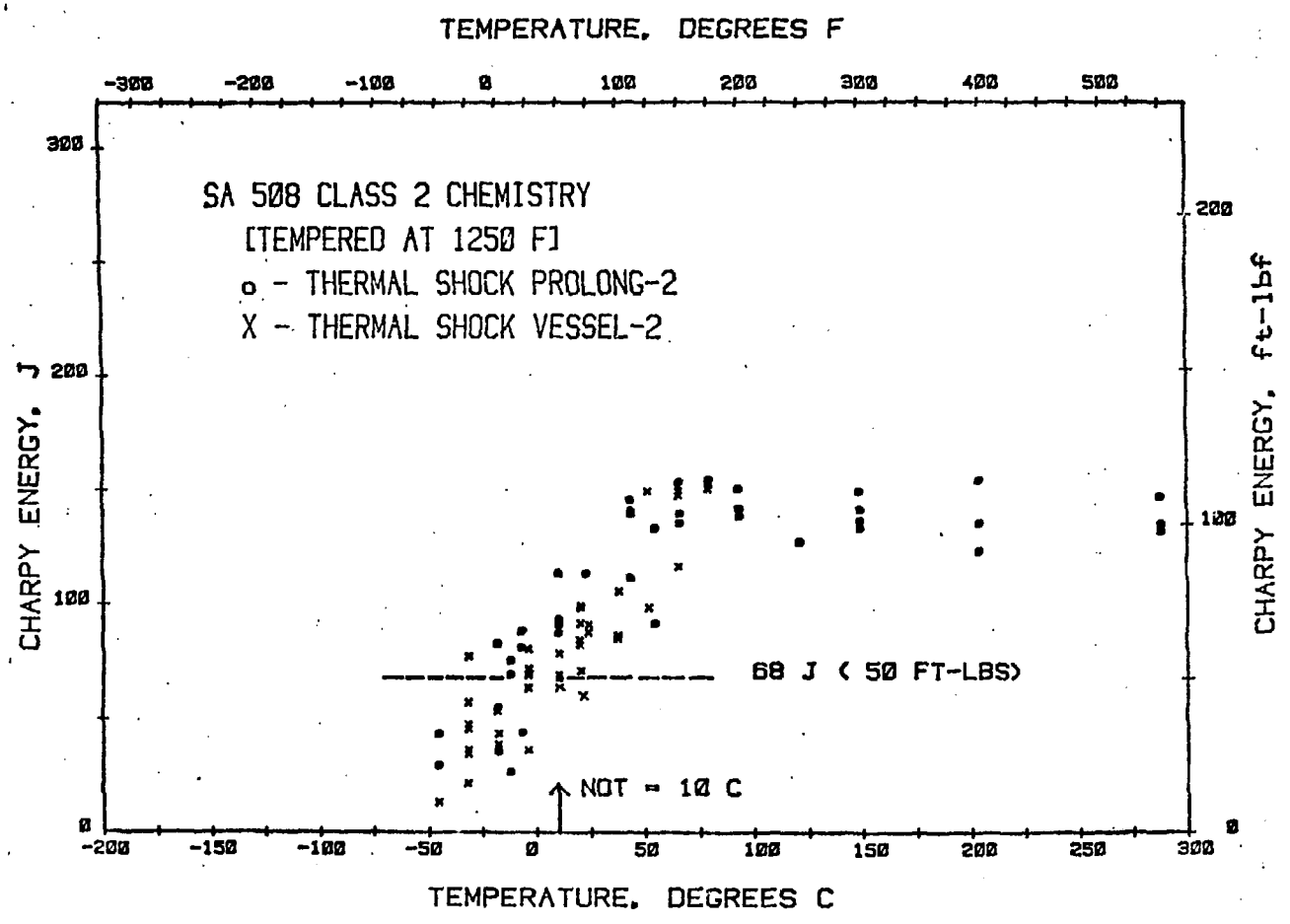

Fig. 6. CVN data for the TSE-5A test cylinder and its prolongation.

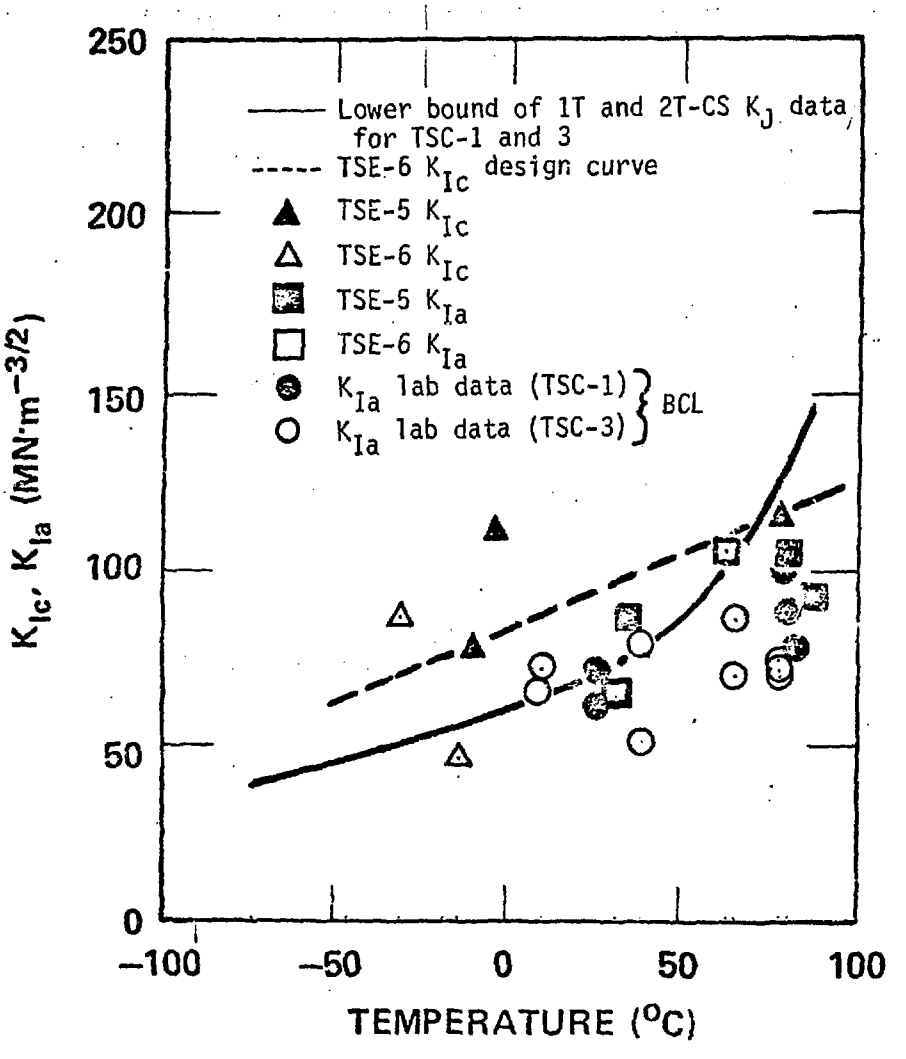

Fig. 7. Comparison of K_{Ic} and K_{Ia} data from TSE-5 and TSE-6 with small-specimen lab data.

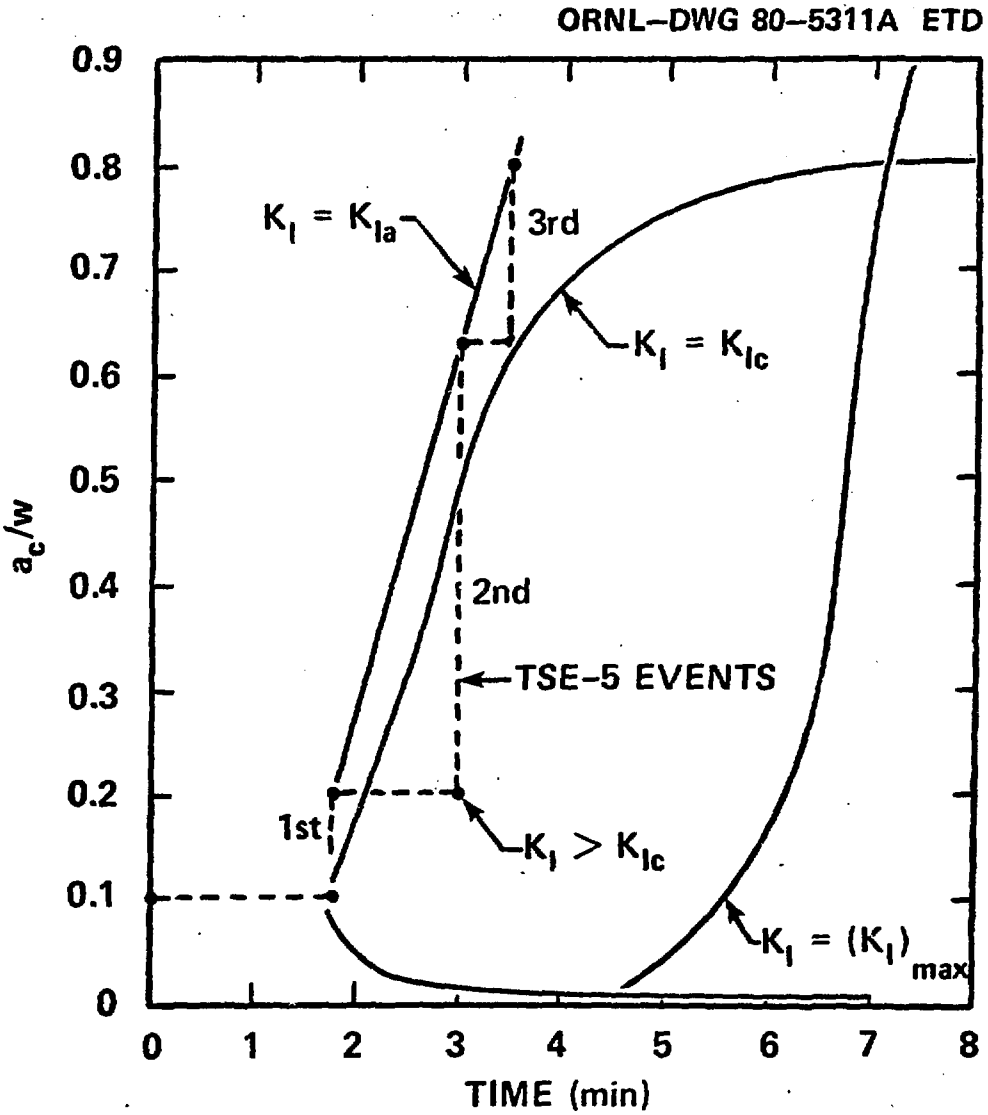

Fig. 8. Posttest critical-crack-depth curves for TSE-5 obtained using a fracture-toughness curve deduced from TSE-5.

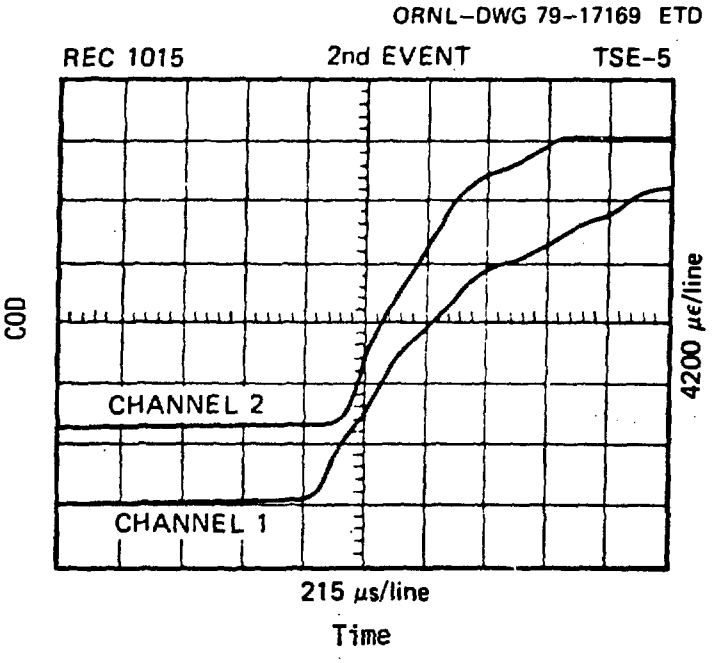

Fig. 9. COD output vs time for second crack jump during TSE-5.

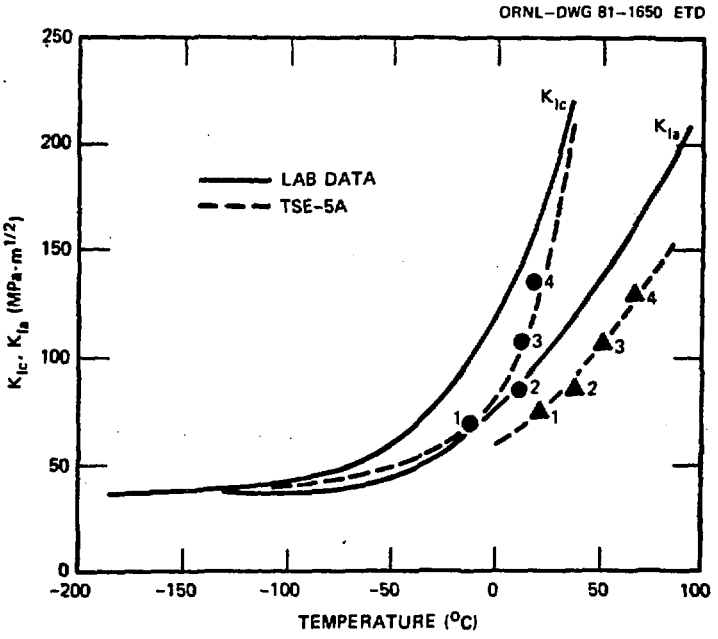

Fig. 10. Comparison of K_{Ic} and K_{Ia} values deduced from TSE-5A with TSE-5A design curves derived from lab K_J and K_{Ia} data (see Fig. 5).

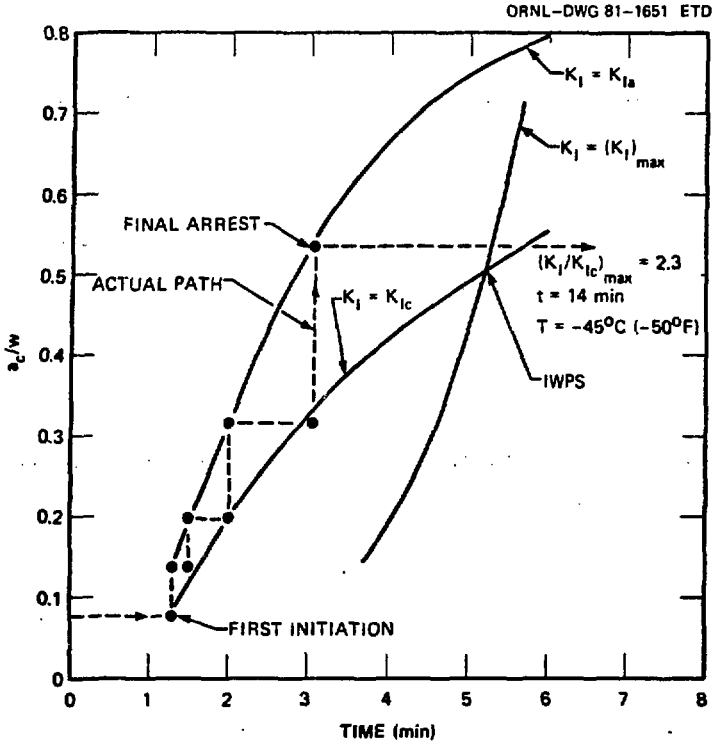

Fig. 11. Posttest critical-crack depth curves for TSE-5A obtained using toughness curves deduced from TSE-5A.

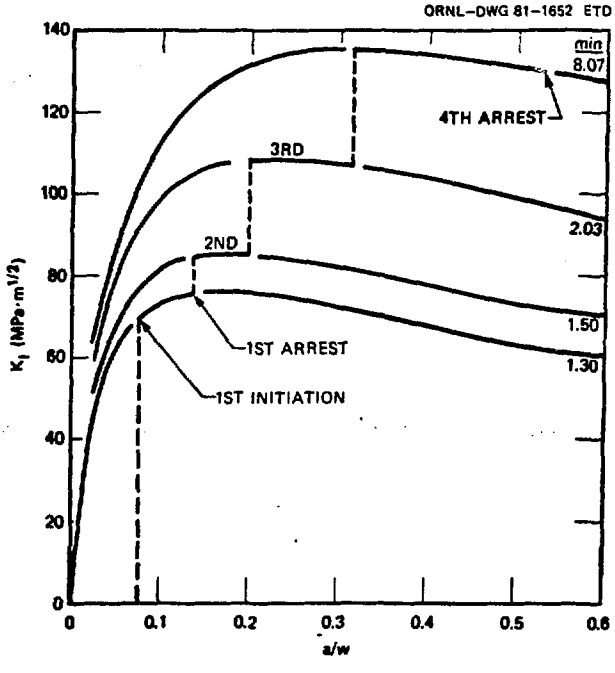

Fig. 12. K_I vs a/w for the times at which initiation-arrest events took place, showing arrest in a rising K_I field for the first event.

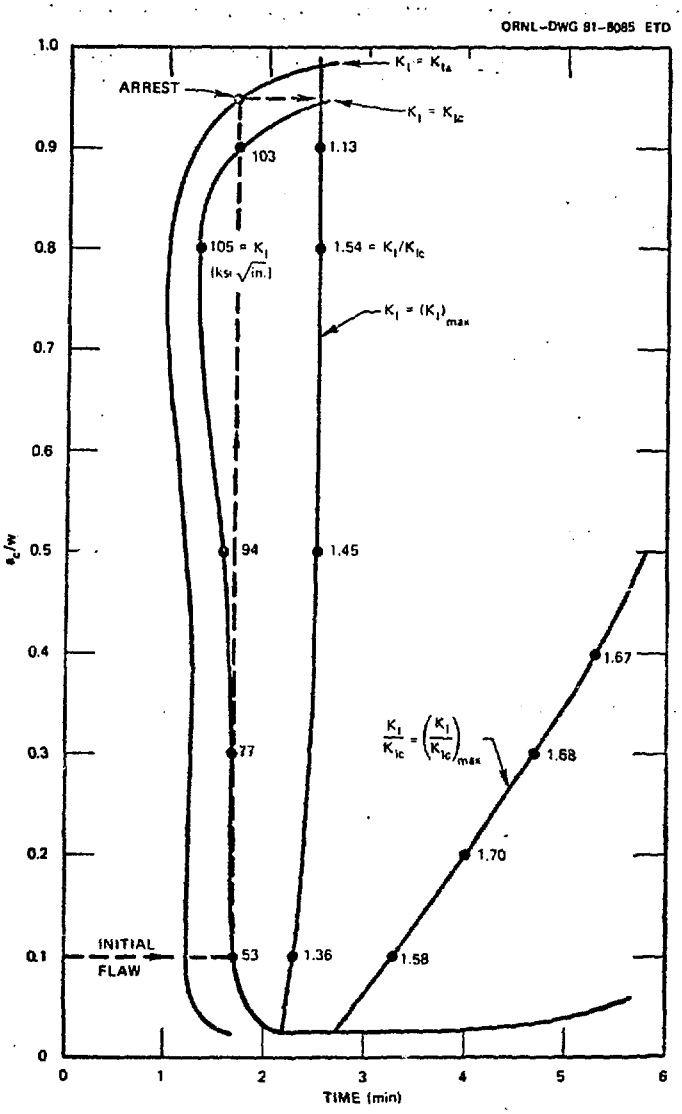

Fig. 13. Pretest critical-crack-depth curves for TSE-6.

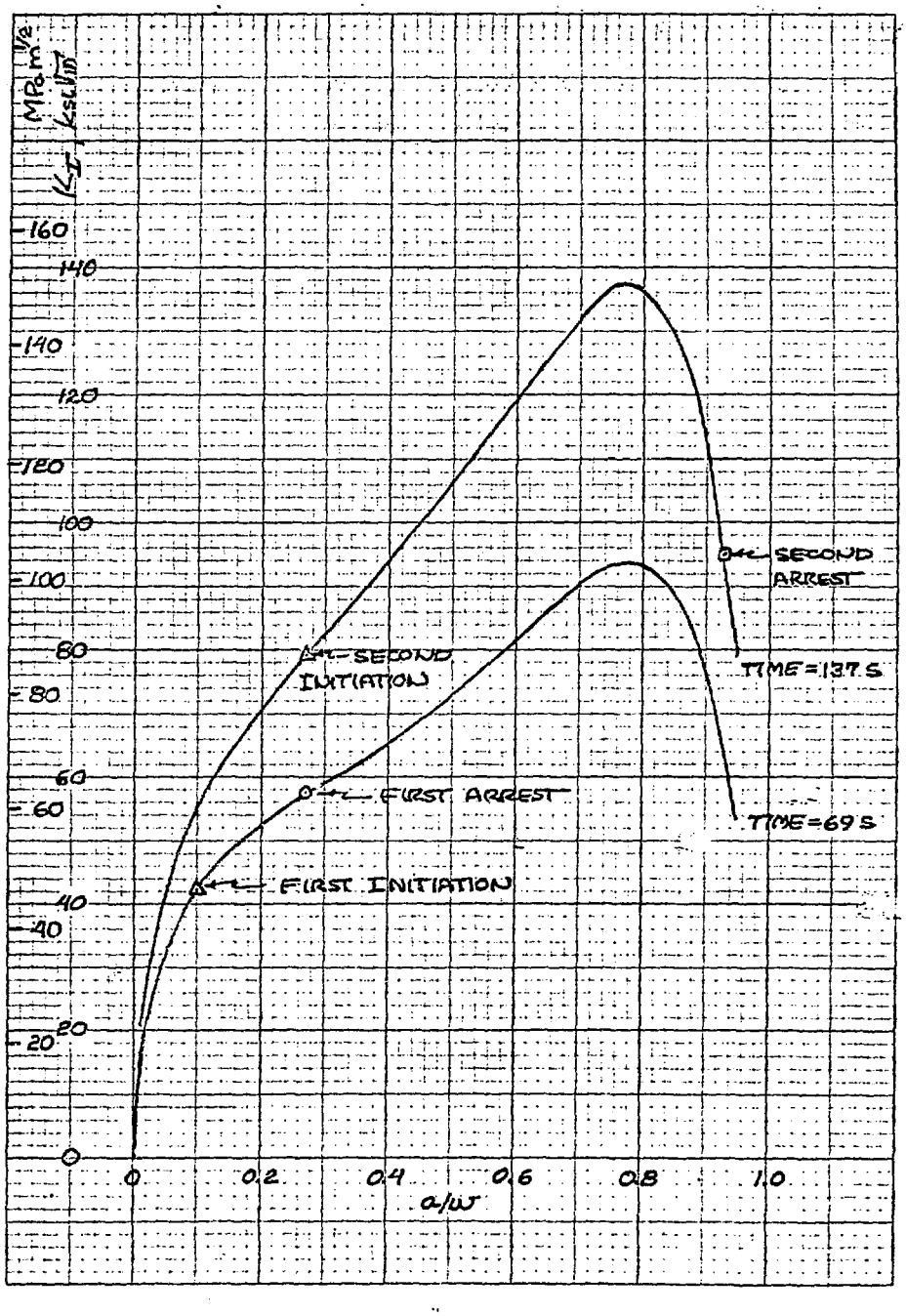

Fig. 14. K_I vs a/w for times corresponding to the two initiation-arrest events during TSE-6.

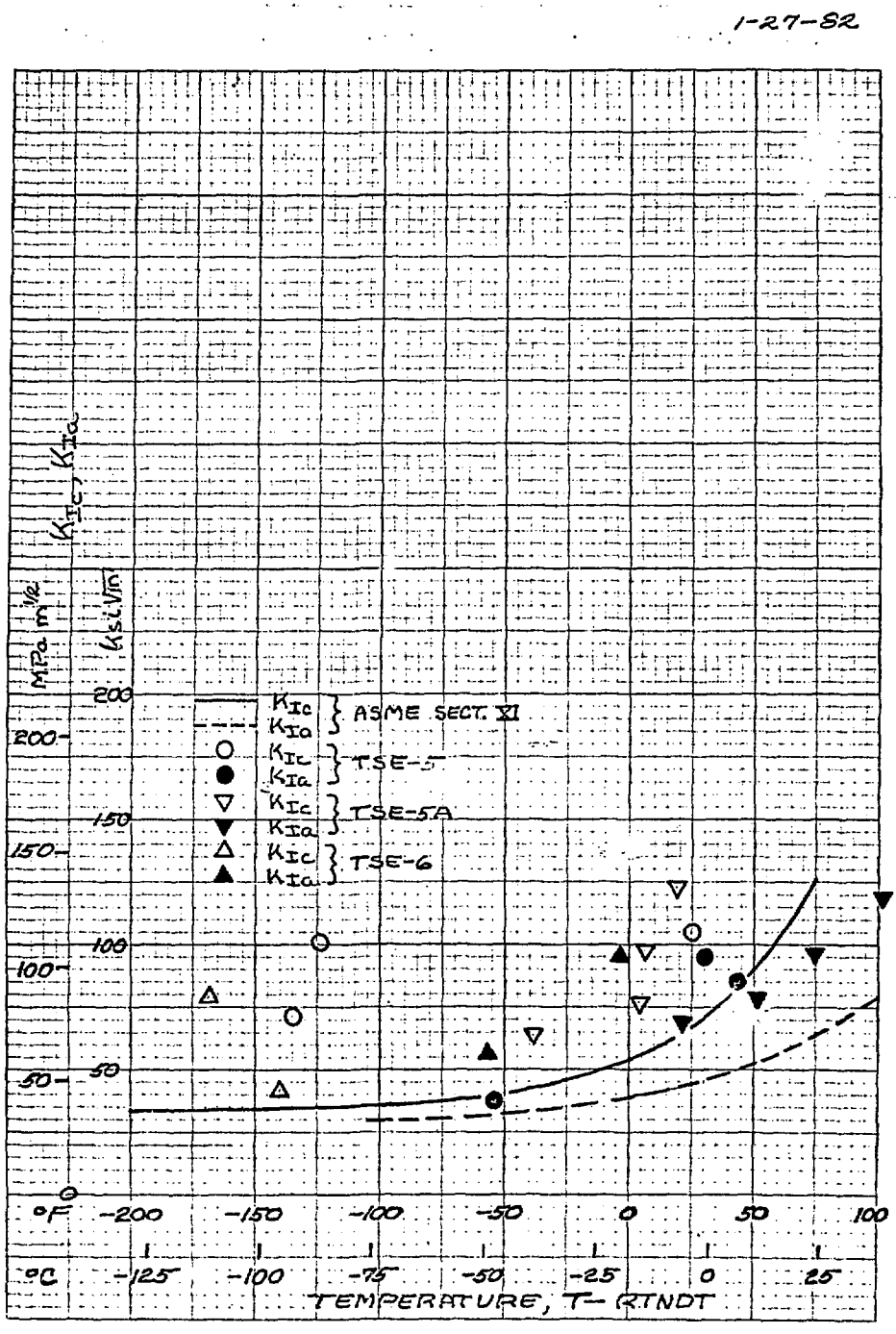

Fig. 15. Comparison of K_{Ic} and K_{Ia} data deduced from TSE-5, 5A and 6 with the ASME Sect. XI K_{Ic} and K_{Ia} curves.